Reviews

Nanographites, their compounds, and film structures

A. M. Ziatdinov

Institute of Chemistry, Far East Branch of the Russian Academy of Sciences,
159 prosp. 100 let Vladivostoku, 690022 Vladivostok, Russian Federation.
Fax: +7 (423) 231 2590. E-mail: ziatdinov@ich.dvo.ru

The current state of the art in the synthesis and investigations of nanographites and their compounds and film structures is reviewed. Considerable attention is focused on the contribution of the edge π-electron states to the physical and chemical properties of nanographites and their compounds. Promising routes to new types of nanographite compounds and film structures are specified. The methods of formation and properties of new nanographite composites are discussed. The nanocarbon systems under consideration are believed to be promising materials for advanced technological purposes.

Key words: nanographite, nanographite compounds, nanographite films, nanographite composites, edge π-electron states, chemical activity.

In the last few years, nanoscale carbon structures with topologically different π-electron "worlds" (fullerenes, nanotubes, graphene, *etc.*) have been extensively studied, both experimentally and theoretically, because of their unique physicochemical properties.[1—4] Another member of this family is nanographene. This is a planar honeycomb carbon structure with a 2D π-electron system and at least one nanoscale lateral dimension (Fig. 1, *a*). A stack consisting of several nanographenes is commonly referred to as nanographite (Fig. 1, *b*). The 2D nanoscale π-electron conjugated system and open edges render nanographene a specific mesoscopic object differing from both infinite graphene and edgeless fullerenes and cylindrical carbon nanotubes in which the terminal atoms negligibly affect their properties. Being intermediates between bulk graphite and aromatic molecules, nanographenes and nanographites are potential sources of novel chemical compounds, including those possessing unusual electronic and magnetic properties. The present review covers the methods for the synthesis, structures, and physical and chemical properties of nanographites and their compounds, films, and composites. In addition, some approaches to the solution of the problems facing the nanotechnologists that deal with these promising objects are discussed.

Electronic and magnetic structures of nanographites

Nanographites are part of many carbon materials, being structural elements (blocks) in some of them.[4—13] Activated carbon fibers (ACF) are structurally a 3D disordered system of nanographites separated from each other

Published in Russian in *Izvestiya Akademii Nauk. Seriya Khimicheskaya,* No. 1, pp. 0001—0014, January, 2015.

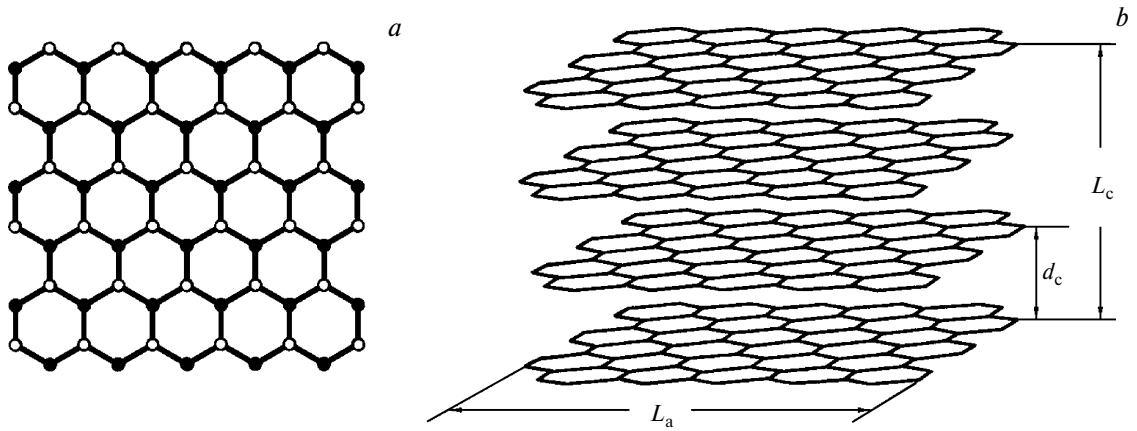

Fig. 1. Schematic representations of idealized nanographene (*a*) and nanographite (*b*) with the armchair and zigzag patterns of adjacent edges. The carbon atoms of different sublattices in nanographene are indicated by full and open circles; L_a and L_c are the nanographite dimensions, d_c is the spacing between nanographenes.

by micropores and the amorphous carbon phase.[4—7] Activated mesocarbon microgranules contain a system of partially ordered nanographites.[5,8,9] Carbon coatings prepared by activation of polymer films show well-oriented nanographite structures.[5,10] High-temperature chlorination of carbides (*e.g.*, SiC, TiC, and B_4C) leaves a carbon framework that is actually a 3D disordered system of nanographenes and nanographites.[5,11—13] In the above carbon materials, nanographites are linked with each other by few functional groups and carbon—carbon bonds of the sp^3-type.[5,14] A system of nanographites without such linkage can be synthesized, *e.g.*, by high-temperature treatment of powdered nanodiamonds under an inert gas.[15] Nanographite-like structures surrounded by many diverse fragments have been found in coals[16] and some kinds of soot.[17—19] Note that nanographene itself (a structural element of nanographite) was first obtained in 2001 by thermal treatment of a nanoscale diamond particle placed on the surface of a graphite plate; its lateral dimensions were ~10 nm.[20,21]

Typical nanographites are 2—10 nm in in-plane size and comprise up to 10—15 turbostratic nanographenes.[4—15] Under normal conditions, chemical substances present in the atmosphere (like oxygen and various compounds with oxygen-containing functional groups) saturate the vacant σ-orbitals of the edge carbon atoms of nanographites. That is why they do not contribute to the electronic structure of nanographite near the Fermi level. Nevertheless, the nanoscale dimensions of the π-electron conjugated system and the considerable specific weight of the surface and edge atoms impart specific properties to nanographite.[4,22—24]

The calculations[22—24] show that the electronic structure of a nanographene ribbon, which is infinite along one direction and has a nanoscale dimension along the other, critically depends on the shape of its edges. Zigzag-edged ribbons are characterized by the edge π-electron states due to the topological features of the π-electrons in zigzag rows of atoms. The energy bands formed by the π-electrons of zigzag edges are partially planar near the Fermi level and, consequently, the density of electron states diagram shows a sharp peak (Fig. 2, *a*). The calculations of the electronic structure of a nanographene ribbon with armchair edges yield no such edge states (Fig. 2, *b*). The charge density in the edge π-electron states is mainly localized at zigzag edges (Fig. 3). The maximum contribution of the edge states to the electronic structure of a nanographene ribbon near the Fermi level is achieved when its width is several nanometers.[23] In this case, ~2% of the total number of the π-electrons in nanographene is concentrated at the Fermi level. However, for a ribbon ~10 nm wide as well, a peak of the density of edge π-electron states near the Fermi level is still quite significant.[23] The presence of some armchair regions in the zigzag edges of a nanographene ribbon diminishes the edge effect on the electronic structure of the ribbon near the Fermi level. Nevertheless, when the fraction of the armchair edges in nanographene ribbons is ~1/3, the energy spectrum still shows an appreciable peak of the density of edge π-electron states at the Fermi level.[23]

Detailed calculations of the electronic structure of a semiinfinite nanographene ribbon with zigzag edges,[4,22,24] which made allowance for electron—electron interactions, yield high magnetic moments on the edge carbon atoms and suggest the possibility of forming an edge ferromagnetic chain (Fig. 4, *a*). At zigzag regions of the nanographene edges of limited size, spin-polarized states can arise (Fig. 4, *b*).[25] According to the calculations,[26] the zigzag edges of nanographene cannot be distorted by electron—phonon interactions unless they are unrealistically strong.

In a stack of turbostratic nanographenes with zigzag edges, the peripheral π-electron states are retained.[25] However, when nanographenes form an array in a stack, their

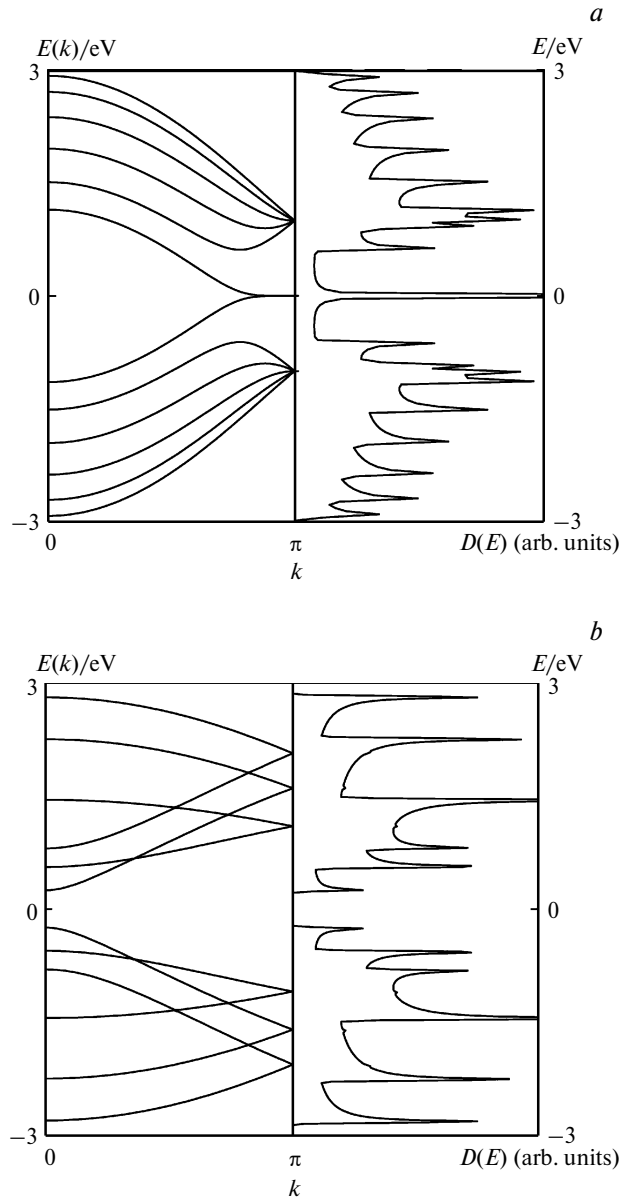

Fig. 2. Band structure plot $E(k)$ and the density of states diagram $D(E)$ for a nanographene ribbon made up of six zigzag (*a*) and six armchair rows (*b*).[23]

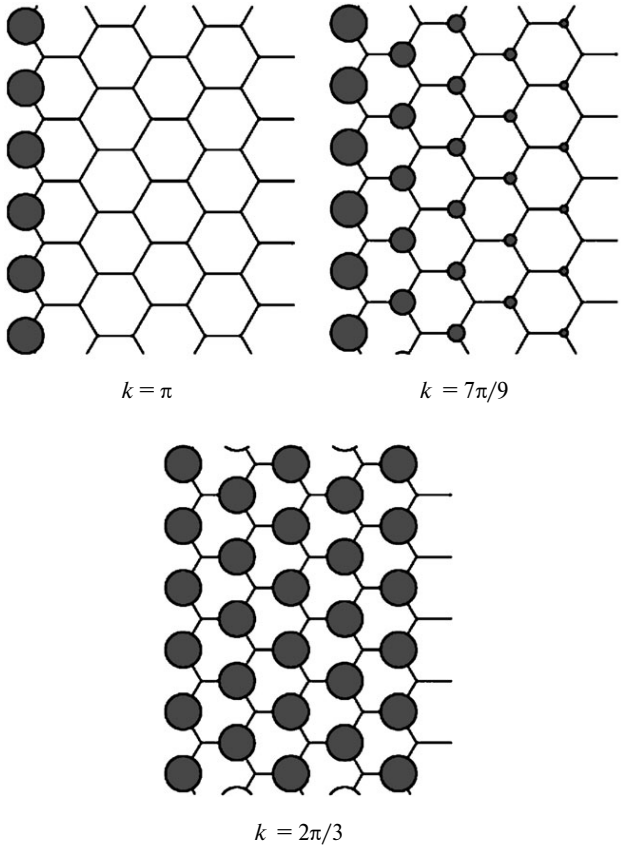

Fig. 3. Schematic representation of the charge density near the zigzag edge of graphene for different values of the wave vector k. The radius of each circle is proportional to the charge density.[22–24]

electronic structure depends on both the number of layers and the packing pattern.[27–29] For instance, a nanographite containing an odd (even) number of identically packed nanographenes shows (no) edge π-electron states.[29]

Despite the aforesaid achievements in the theoretical studies of the π-electron states at the edges of honeycomb carbon networks, there is still no generally recognized estimate of the energy ratio for their armchair and zigzag regions.[30–33] This precludes any prediction of the structural motifs of the edges of real carbon networks, especially when they are part of more complex carbon structures. There is no technology so far for growing carbon networks with required edge patterns, although extensive research in this field has already provided some encouraging results.[34,35] For this reason, current experiments aimed at revealing the edge π-electron states and studying their effect on the properties of one or another carbon structure are mainly dealing with objects having their inherent edge patterns.

Direct experimental evidence for the presence of a peak of the density of π-electron states near the zigzag edges of a honeycomb carbon network has been obtained by scanning tunneling spectroscopy (STS).[36–41] Prior to this, the zigzag edge regions themselves of the carbon structures had been identified by scanning tunneling microscopy (STM).[36–41] The STM and STS techniques were used[36] to examine the edges of one-atom-thick terraces on the surface of graphite crystallites ~150 nm in size. Such crystallites are produced, *e.g.*, by thermal expansion of a plate of highly oriented pyrolytic graphite (HOPG) with intercalated HNO_3. The same techniques were used to examine[37] the edges of nanographenes grown on the surface of a HOPG plate from nanodiamonds subjected to special thermal treatment as well as the edges of a honeycomb

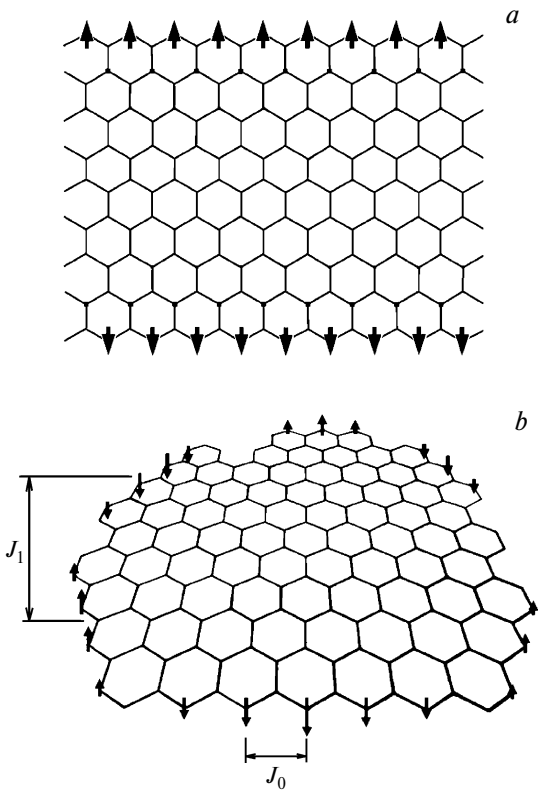

Fig. 4. Schematic representation of an edge ferromagnetic structure in nanographene: (*a*) a semiinfinite nanographene ribbon with zigzag edges[22] and (*b*) a nanoscale part of graphene with some zigzag edges;[25] J_0 and J_1 are the exchange interactions inside and between the zigzag regions of the edges, respectively.

carbon network grown on the surface of polycrystalline iridium.[38] Near the zigzag edge regions in the carbon structures studied,[36—38] the local density of π-electron states is manifested as a well-defined peak whose energy is lower by 25±5 meV than the Fermi energy. Such a peak was not revealed near the armchair edges of those carbon structures.[36—38]

An STM examination of multiple-atom vacancies in graphene bombarded with Ar^+ showed that their edges also have extended zigzag regions at which edge π-electron states arise and persist even upon protonation of the edge atoms (Fig. 5).[39,40] Near the protonated edges of the defect, an STS study revealed two peaks of the local density of π-electron states (somewhat higher and lower than the Fermi energy) probably caused[39,40] by spin splitting of the edge π-electron states. These findings agree with the data for the local density of electron states near the oxidized zigzag edges of a microscale honeycomb carbon network.[41] However, in the latter case, the minimum inward distance from the sample edge that suffices to "quench" the excess density of π-electron states is approximately ten times longer than the corresponding distance from the protonated edges of the multiple-atom defect.[39—41] This

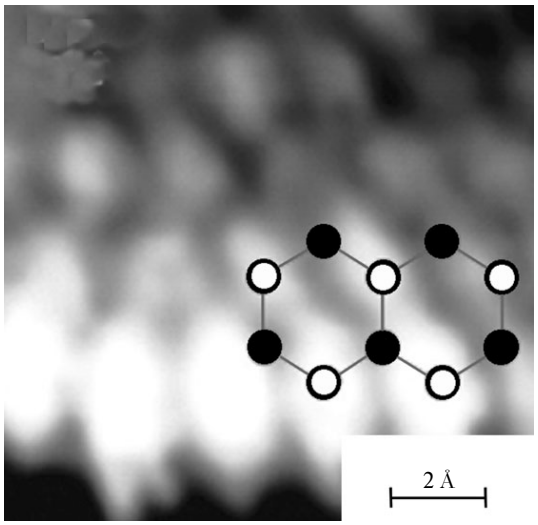

Fig. 5. STM image of the zigzag edge of a multiple-atom vacancy in graphene.[39] The brightness of every spot is proportional to the local density of π-electron states.

distinction suggests that the oxygen atoms in functional carbonyl groups at the edges of a carbon network serve as additional π-centers.

The edge π-electron states are also found in nanographites. This is evidenced by, *e.g.*, ESR data and static magnetic susceptibility measurements of ACF[42,43] as well as by analysis of near-threshold fine structures in the X-ray absorption spectra of various nanographite compounds.[44—46]

The ESR spectrum of ACF shows two signals having equal *g*-factors but largely different widths (Fig. 6, inset).[42,43] With a decrease in the temperature, the integral intensity of the wider signal remains unchanged (Fig. 7, *a*), while that of the narrower signal roughly obeys the Curie law (Fig. 7, *b*).[43] Therefore, the wider signal can be attributed to a conduction electron spin resonance (CESR),

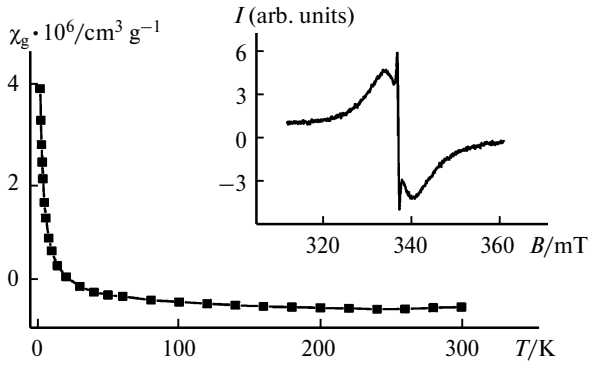

Fig. 6. Plot of the specific magnetic susceptibility of ACF *vs.* the temperature.[42] The points refer to the experimental values; the solid line obeys the equation $\chi_g = 1.318 \cdot 10^{-5}/(T + 0.9) - 0.61 \cdot 10^{-6}$. The ESR spectrum of the same sample at 120 K (inset).[42]

while the narrower one, to a resonance of localized magnetic moments. The integral intensity of a CESR signal is known[47] to be proportional to the carrier density at the Fermi level. The concentration of localized spins can be accurately determined with consideration of low-temperature data on the static magnetic susceptibility of ACF (see Fig. 6). Knowing these data and comparing the intensities of diverse resonance signals, one can easily estimate the carrier density at the Fermi level in nanographites, which are structural blocks of a sample. Such calculations[42,43] give the density of states which is more than 10 times that in bulk regular graphite and agrees well with the densities calculated for nanographenes and nanographites with zigzag edges.[4,22—25] Nevertheless, for nanographites with their inherent edge patterns, this density estimate seems to be surprisingly high. This can be due to the lower energy of the zigzag edges of nanographite compared to its armchair edges. This assumption finds support in experimental data. For instance, graphenes[48] and nanographenes[49—51] grown on certain metal substrates have predominantly zigzag edges. In addition, a study of the multiple-atom vacancy edges in graphene by atomic-resolution electron microscopy revealed that the armchair edges turned zigzag with time.[52] Also note that in the context of the electronic structure model of nanographite with edge π-electron states, some decrease in the integral intensity of a CESR signal (the density of electron states at the Fermi level) of nanographites, which occurs when evacuated ACF comes in contact with the atmosphere (see Fig. 7, *a*),[43] can be explained by spin splitting of the edge π-electron states initiated by electron—electron interactions, which become stronger as the Fermi energy of the particle shifts to the value corresponding to the peak of the density of its edge states.

The presence of a peak of the density of π-electron states near the Fermi level of nanographites is confirmed by the shape of a near-threshold fine structure in the X-ray absorption spectrum of their powders and agglomerates.[44—46] For instance, the spectrum of powdered nanographite ribbons consisting of 2—40 layers 20—30 μm long and 20—300 nm wide shows, on the lower-energy branch of the band due to the transitions from the C1s level to the delocalized π*-electron states, a peak with an energy only slightly differing from the Fermi energy of graphite.[44] Similar features are observed in the corresponding spectra of nanographites in ACF (see Ref. 45) and nanographenes obtained by annealing of a hydrocarbon material deposited from the vapor phase onto a platinum plate.[46]

When analyzing the data for nanographite systems, the authors of the above studies focused on the electronic structure and properties of an individual nanoparticle. However, in some cases, the same data provide important information on the properties of the system of nanoparticles itself. For instance, the possibility of describing the temperature dependence of the magnetic susceptibility of ACF by the Curie—Weiss law with a small negative Weiss constant suggests a weak antiferromagnetic interaction between fiber-localized spins.[42,53,54] Since the edge π-electron states of nanographite below ~1600 °C contain about one unpaired electron,[54] one can believe that the interaction in question occurs between the spins of electrons on different particles. This weak interaction at low temperatures can dramatically change the magnetic structure of a nanographite system.[53,54] For instance, when ACF annealed in an inert atmosphere at the temperature of the metal—insulator percolation phase transition (~1200 °C) is cooled, their magnetic susceptibility plotted versus temperature shows a break[54] (at 4—7 K) characteristic of a spin glass transition.[55] Therefore, a spin glass phase can appear in ACF below these temperatures.[53,54]

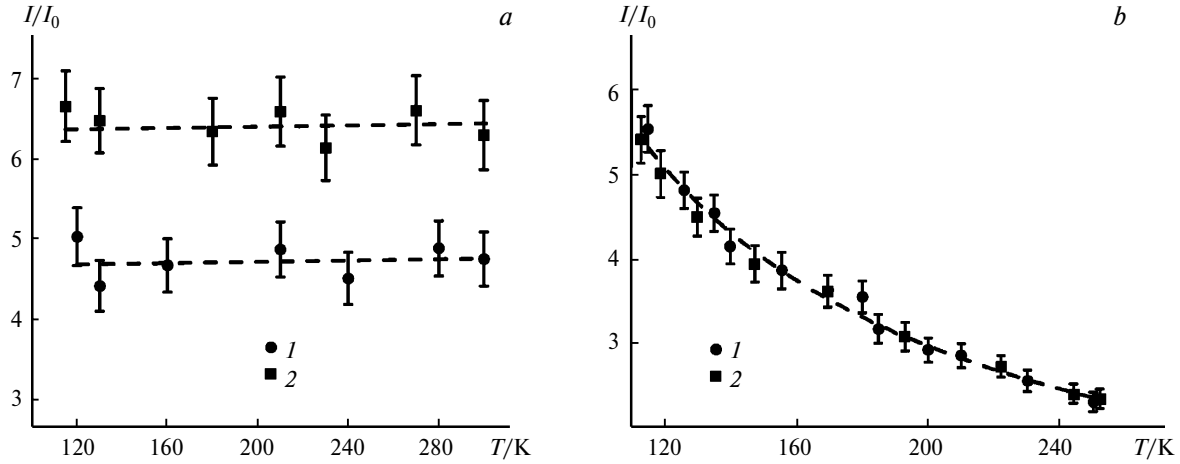

Fig. 7. Plots of the integral intensities of the wide (*a*) and narrow ESR signals (*b*) of ACF *vs.* the temperature:[43] (*1*) the initial sample and (*2*) the evacuated sample; I_0 is the intensity of the ESR signal for a standard. The dashed lines are drawn only for convenience.

Nanographite films and composites

The investigations of nanographenes and nanographites discussed in the preceding section were initiated by the intriguing results obtained in the calculations of their electronic structures. Also, experimental studies aimed at searching for those properties of nanographite films[56–69] and composites[70–74] that would be promising for their practical application (but do not result immediately from the calculations of the electronic structures of nanographites) have been developed in the last few years. The most notable advances in this field have been made when studying interactions of nanographite films obtained by plasma-enhanced chemical vapor deposition from a mixture of methane and hydrogen onto a silicon substrate with the strong electromagnetic field of a laser radiation.[56–58] Specifically, the films have been found to exhibit nonlinear optical properties in such a field.[56,57] These properties can be used to design fast-acting photodetectors of laser radiation and terahertz generators. There is some progress in the use of the photovoltaic effect in nanographite films for designing analyzers of laser radiation polarization as well as sensors of the angular position of a polarizer.[58] Nanographite mesoporous films have been employed as cold emitting cathodes for making prototypes of cathode-luminescent light sources whose characteristics are superior to those of the best known LED samples.[59,60] The undoubted advantage of such light sources is also that their radiation can be colored in any color by adding appropriate phosphors to a nanographite film.[60] Investigations[61–63] of a nanographite film (one to several micrometers thick) grown on a quartz substrate by chemical vapor deposition have shown that its electrical resistivity jumps by four to five orders of magnitude when the strength of an applied electric field reaches some fixed value. This feature of such films can be used to design contactless current limiters and smart chips.[61] In the metastable high-resistance state, these films can be employed as active elements for segmented semiconducting radiation detectors; they can be more sensitive by two to three orders of magnitude than their counterparts based on bulk sensors.[61] A nanographite film in the high-resistance state emits light for a while,[61,62] as observed earlier in semiconducting carbon fibers under similar experimental conditions.[75] Nanographite films can absorb and convert a microwave electromagnetic field into a direct current.[63] Thus, they are promising subjects of further investigations of their applicability in detectors of microwave fields. In the studies discussed above,[56–63] graphite particles in films were only several nanometers in width; however, their average lateral dimensions are much greater than those of nanographite ($l_a \approx 3$ nm), for which the theory predicts a maximum contribution of the edge π-electron states to the electronic structure near the Fermi level.[23] For this reason, the amazing properties of these films cannot unambiguously be attributed to the edge π-electron states. Therefore, it is important to continue investigations aimed at growing film structures of graphite particles with lateral dimensions close to l_a and studying their properties.

In a promising method of growing a nanographite film from a stable dispersion of graphite particles prepared by fragmentation of natural graphite with high-energy ultrasound in various solvents, the average lateral dimension of a graphite particle in the resulting film is of the order of several hundreds of nanometers.[64] In a film grown on a glass plate exposed to an aqueous dispersion of colloidal nanographite (prepared electrochemically with simultaneous exposure of the solution to high-energy ultrasound), graphite particles consist of several turbostratic nanographenes with an average lateral dimension of ~80 nm; note that the electrical resistivity of this film is highly sensitive to low concentrations of NO_2.[65] Nanographite films with the smallest known average lateral dimension of graphite particles (~3 nm) have been obtained from activated carbon materials.[66–69] Specifically, such films have been grown by evaporation of a lyosol of nanographites on various substrates. The lyosol had been prepared by ultrasonic disintegration of ACF (with preliminary removal of their functional groups at high temperatures *in vacuo*) in diverse fluids (Fig. 8).[68,69]

Addition of nanographites as a filler to various matrices can substantially change their inherent properties as well as produce a composite with qualitatively new characteristics.[70–74] Functionalization of a mesoporous carbon foam with nanographites enhances the electrical conductivity of its percolation network and transforms it into a composite electrode material promising for use in double-layer capacitors and lithium ion cells.[70] Nanographite covered with a thin film of iron and nickel codeposited on its acid-functionalized surface effectively absorbs a microwave field from 300 MHz to 1.5 GHz; because of this, this nanographite is of interest for various defense applica-

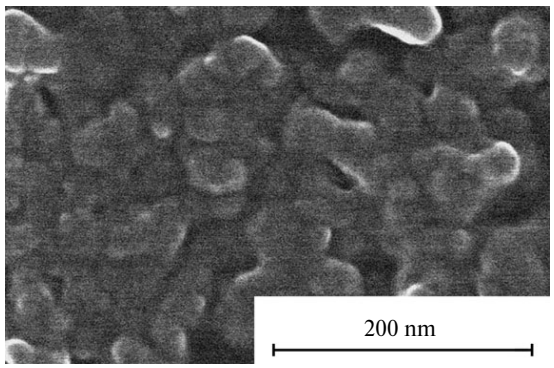

Fig. 8. Micrograph of a nanographite film grown by evaporation of a lyosol of nanographites on a silicon substrate.[69]

tions.[71] Addition of nanographites to phase-change materials improves their heat conductivity,[72] which is important for energy storage technology using such materials. Addition of nanographites to the prepregs of carbon-carbon composites affects the properties of the final carbonized product.[73] A low content (<1.5 wt.%) of nanographite in the prepregs enhances their mechanical characteristics by tens of percent, whereas a high content of nanographites deteriorates the same properties of the final product. It is believed that the deterioration of the properties of a material containing high amounts of nanographite is caused by agglomeration of its nanoparticles, which precludes them from filling the pores of the carbon-carbon composite.[73] It is also worth noting that the increased sensitivity and stability of electrodes modified with carbon nanotubes with respect to phenol and *p*-cresol, which is well known to electrochemists, are really not inherent in the nanotubes themselves (as believed earlier), but rather associated with nanographite impurities introduced into the electrodes with the nanotubes.[74]

Nanographite compounds

Nanographite can form, depending on the nature of the reagents and the reaction conditions, both covalent[44,45,76–79] and charge transfer compounds.[80–83] With certain reagents, nanographite forms "mixed" compounds showing covalent carbon—reagent bonds at the periphery of a nanoparticle and charge transfer compounds in its bulk.[45,81,82]

There are two known types of covalent compounds of nanographite: (1) compounds in which covalent carbon—reagent bonds are mainly formed by edge carbon atoms (an edge covalent compound of nanographite, Fig. 9, *a*) and (2) compounds in which such bonding occurs throughout the bulk of a sample (a bulk covalent compound of nanographite). The reason why covalent compounds of nanographite can exist in two types is that the edge carbon atoms of nanographite have unsaturated σ-orbitals and thus are chemically more active than its bulk carbon atoms containing no such orbitals. The chemical activity of edge carbon atoms has been reported[84] to depend on the configuration of the positions they occupy: at zigzag edges, they are more active than at armchair edges. The difference in chemical activity between the edge and bulk carbon atoms of nanographite enables one to select such conditions for the synthesis at which the covalent carbon—reagent bonding proceeds in two steps: first, such bonds are mainly formed at the periphery of nanoparticles, whereupon, by changing some conditions, these are made to form in the bulk. Note that theoretical analysis of the fluorination of nanographene also suggests the possibility of a two-step reaction: first at the edges of a nanoparticle and then in its bulk.[85] To date, edge covalent compounds of nanographite with hydrogen,[25,39,76] fluorine,[45,77] and chlorine[77] have been identified and examined. It has been assumed[81,82] that nanographite also forms such compounds with bromine and iodine. However, only two bulk covalent compounds of nanographite with fluorine[45,77] and oxygen[78,79] have been identified and studied hitherto.

The edge covalent compound of nanographite with hydrogen is best known and relatively easy to prepare. This compound is usually synthesized by exposure of nanographites with defunctionalized edges to a hydrogen atmosphere at ~1000 °C for 1 h and longer.[25,39,76] The free σ-orbitals of the edge carbon atoms become saturated and,

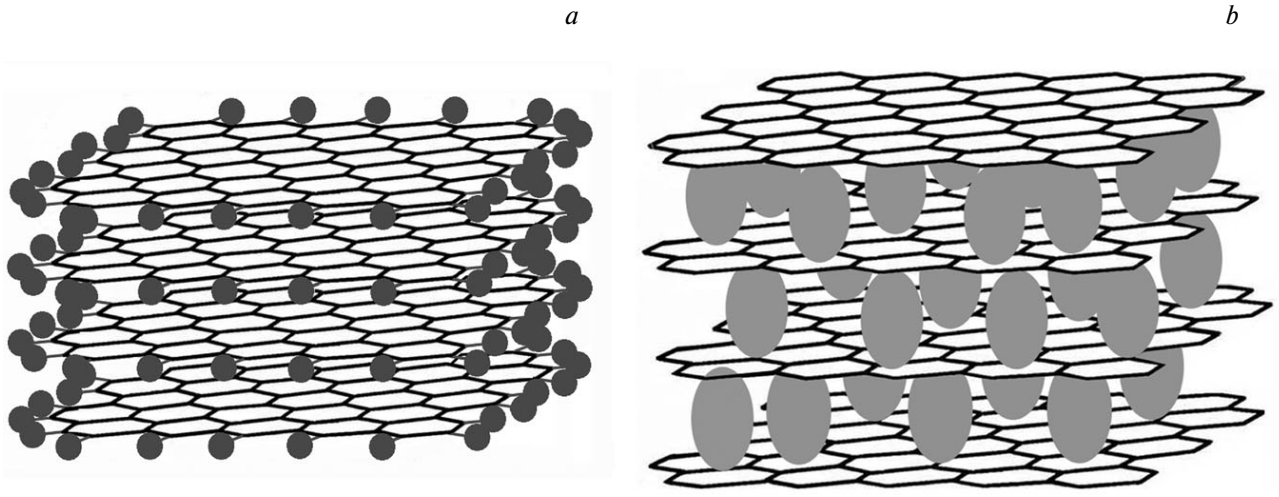

Fig. 9. Schematic representation of an edge covalent nanographite compound (*a*) and a nanographite intercalation compound (*b*); the intercalated atoms (molecules) are indicated with circles and ellipses, respectively. The size ratios of the carbon network and the reagent atoms (molecules) are arbitrary and only serve to make the pictures clearer.

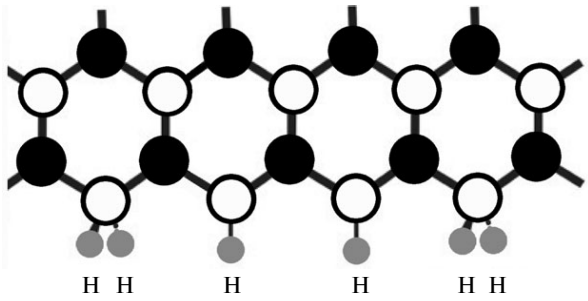

Fig. 10. Schematic representation of a chain structure in the protonated zigzag edge of a multiple-atom vacancy in graphene.[39]

consequently, the associated paramagnetism disappears. The edge carbon atoms can be bound to both one and two hydrogen atoms.[39,86] According to the calculations[86] and the STM data,[39] such bonds make a periodic pattern (Fig. 10) rather than alternate randomly.

Nanographite reacts with fluorine to give both edge and bulk covalent compounds.[45,77] Analysis of the near-threshold fine structure of the X-ray absorption spectrum, the ESR data, and the static magnetic susceptibility for products of a room-temperature reaction of gaseous fluorine with ACF shows that the halogen atoms at $F/C \leq 0.4$ are covalently bound mainly to the edge atoms of nanographites (structural blocks of a sample).[45] In this fluorination step, the concentration of localized spins decreases because of the saturation of vacant σ-orbitals of the edge carbon atoms. At $F/C > 0.4$, fluorine also attacks the bulk carbon atoms of nanographites. As a result, a carbon atom adjacent to that attacked by fluorine gets a vacant (unsaturated) σ-orbital with a localized spin.[45] The concentration of spins localized on such orbitals is maximum at $F/C \approx 0.8$. Above this value, covalent bonds are predominantly formed between the fluorine atoms and the bulk carbon atoms of nanographites having vacant σ-orbitals. This process stops at $F/C \approx 1.2$, which is evidenced, in particular, by disappearance of the ESR signal for localized spins.[39]

ACF can also be fluorinated with gaseous BrF_3 produced by thermolysis of $Na[BrF_4]$.[77] In this case, the degree of fluorination of nanographites in ACF is mainly temperature-dependent. The X-ray photoelectron spectrum of the C1s electrons of ACF fluorinated at ~155 °C shows a line of carbon bound to one F atom. The integral intensity of this line is 25—30% of the total integral intensity of the spectrum of the C1s electrons and is consistent with the percentage of the edge carbon atoms in an idealized round nanographene particle ~1.6 nm in diameter. Fluorination of ACF at ≥300 °C yields nonconducting compounds of nanographites similar in composition to digraphite monofluoride $(C_2F)_n$ thought[87] to be made up of corrugated layers of sp^3-hybridized carbon that are "crosslinked" in pairs.

According to the data from X-ray photoelectron spectroscopy and X-ray diffraction, the product of a room-temperature reaction of ACF with chlorine for all the halogen concentrations used shows covalent chlorine—carbon bonds mainly at the periphery of nanographites.[77] These bonds are relatively stable and withstand heating up to ~150 °C. The concentration of localized spins in ACF, which was determined by ESR, decreases by one third with an increase in the chlorine content. This agrees well with the data on the covalent bonding between the halogen and the edge carbon atoms under these conditions.

Analysis of the weight changes for nanographite agglomerates and powders in the adsorption of bromine and iodine molecules followed by their desorption from the evacuated samples shows that the adsorption is not completely reversible for $Br/C > 0.27$ and $I/C > 0.32$.[81,82] Comparison of the measured static magnetic susceptibility for the samples with reversible and irreversible halogen adsorption suggests that the concentration of localized spins in the former is greater by a factor of three to five than that in the latter. Raman spectroscopy studies of the samples in different adsorption and desorption steps have revealed no changes in the average sizes of nanographenes.[81,82] All these facts provide evidence for covalent bonding between carbon atoms and some of the adsorbed halogen atoms. Obviously, covalent bonds are most likely formed at the edges of nanographites and of the structural defects in the bulk of nanoparticles.

In nanographene, the π- and σ-orbitals of the carbon atoms are mutually orthogonal; for this reason, saturation of its vacant edge σ-orbitals should seemingly not affect the state of the π-electrons. However, the ESR data[45,77,81,82] for the products of the reactions of ACF with halogens suggest that the covalent bonding between halogen atoms and the peripheral carbon atoms of nanographites is accompanied by the changes in both the *g*-factor and the spin relaxation rate of the π-electrons (Fig. 11). These changes can be attributed to the transformation of the edge π-electron zone as well as to the $sp^2 \rightarrow sp^3$ transition for some peripheral orbitals upon the saturation of the edge σ-orbitals.[39,41]

Nanographite oxides can be prepared using oxidation of thermally expanded graphite, activation of epoxy and ether groups of graphite oxide with chloroacetic acid, treatment of the activated product with high-energy ultrasound, and disintegration.[78] Nanographite oxide has also been obtained by hydrothermal synthesis from superdispersed graphite.[79] According to the data obtained,[78,79] nanographite oxide, regardless of the method of its preparation, is well soluble in water, exhibits visible to IR photoluminescence, biocompatible, and suitable as a vehicle for drug delivery to particular cancer cells. Note that nanographites can be made hydrophilic not only by their transformation into covalent graphite oxide but also simply by emul-

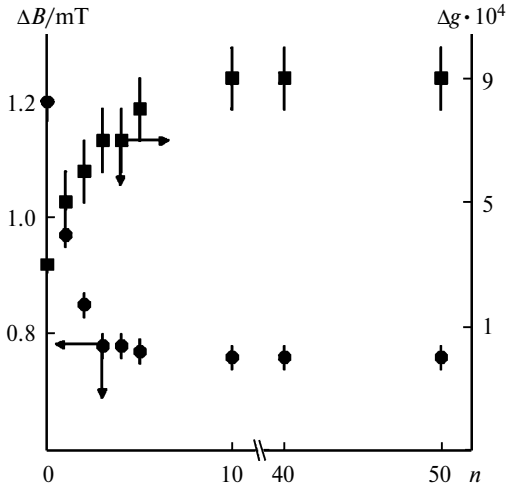

Fig. 11. The width ΔB and the shift of the g-factor ($\Delta g = g - g_e$) of the CESR signal in ACF as functions of the number n of chlorine portions added together with the sample to the reactor;[77] ΔB is proportional to the spin relaxation rate of the carriers;[47] $g_e = 2.0023$ is the free-electron g-factor.

sion polymerization at their surfaces (*e.g.*, with methacrylate as a starting monomer[88]).

It is well known[89] that nanoparticles can have unusual magnetic structures and exhibit such magnetic properties that are absent from their macroscopic analogs. According to the calculations,[90–92] the ground state of a nanographene ribbon in which the opposite zigzag edges are chemically different (see, *e.g.*, Fig. 12) can be magnetic. However, this intriguing theoretical prediction has not been confirmed hitherto by reliable experimental data because, among other reasons, of unsolved problems of the synthesis and identification of such compounds. One can assume that they can form when chemically modified ACF (*i.e.*, fibers consisting of nanographites with carbon—noncarbon covalent bonding for the overwhelming majority of their edge carbon atoms) are irradiated by low-energy ions like protons, B^+, and Ar^+.[70] Obviously, since the orientations of the nanographite edges relative to the direction of ion bombardment are different, there is some probability in such experiments that these edges will differ in chemical state.

Let us now consider nanographite intercalation compounds (NGIC) formed by charge-transfer reactions of nanographites with molecules intercalated between their carbon layers (see Fig. 9, *b*). It is known that bulk graphite forms charge-transfer complexes with some substances but does not with others (even if the latter are known to react with polycyclic aromatic hydrocarbons to give charge-transfer complexes). For instance, graphite and iodine do not combine to yield a charge-transfer complex,[93] though such a complex has been reported for iodine and perylene.[94] Since nanographite is structurally "intermediate" between polycyclic aromatic hydrocarbons and bulk graphite, its reactivity is difficult to predict with reference only to the known chemical properties of bulk graphite and polycyclic aromatic hydrocarbons.

Investigations dealing with the synthesis of NGIC and their physical and chemical properties are few so far. The product of a reaction of ACF with iodine has been studied by Mössbauer spectroscopy.[80] The spectrum provides evidence for the presence of both neutral iodine molecules and a small amount of I_3^- ions; *i.e.*, some adsorbed iodine molecules are involved in a charge-transfer reaction with nanographites. Therefore, nanographite in the reaction with this halogen is a stronger electron donor than bulk graphite. Detailed examination of products of a reaction

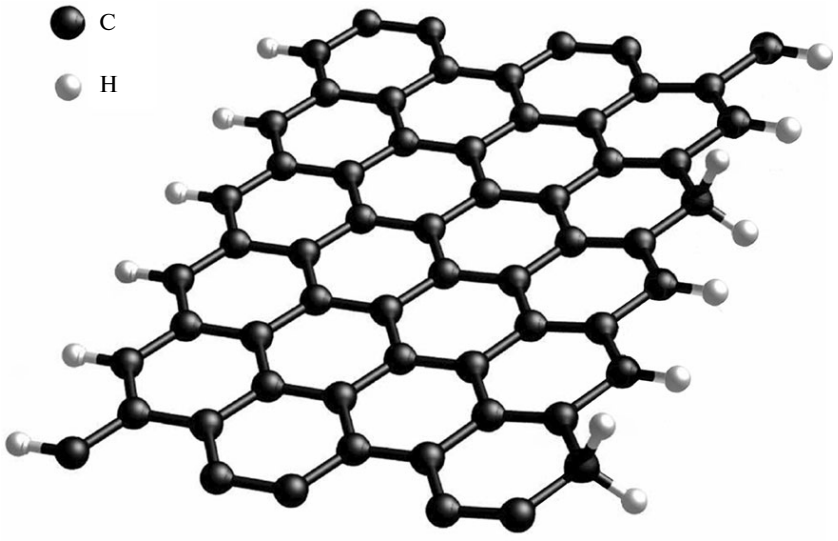

Fig. 12. Schematic representation of nanographene in which the opposite zigzag edges are chemically different.

of powdered nanographites with iodine molecules by different physical techniques shows[81] that the limiting size of nanographene below which iodine does not react with the nanoscale π-electron conjugated system and, consequently, does not intercalate into nanographite is ~6 nm. However, even in the formation of NGIC with iodine, the charge transfer from the carbon network to the intercalated molecule is low (*e.g.*, its value in a $C_{65}I$ sample is an electron per ~2000 carbon atoms[81]). For comparison, the charge transfer in single-walled carbon nanotubes with intercalated iodine is an electron per ~55 carbon atoms.[95]

When bromine molecules are reversibly sorbed by ACF from a liquid phase, some of them are also involved in a charge-transfer reaction with the outer layers of nanographites and intercalate between their carbon layers to produce NGIC with a formula of $C_{38}Br$.[81,82] In reactions of nanographite and bulk graphite with bromine under the same conditions, the charge transfer in the former is substantially lower than that in the latter (an electron per ~2500 (see Refs 81, 82) and ~500 carbon atoms,[93] respectively). In this case, nanographite is a weaker electron donor than its macroscopic analog.

Bulk graphite shows the characteristic tendency to form intercalation compounds with different stage numbers when reacting with the same substance (the stage number is the number of graphite layers sandwiched between the nearest intercalated layers[93]). The formation of NGIC with different stage numbers has been detected hitherto only for nanographite compounds with potassium.[82] According to X-ray diffraction data, the product of a reaction of powdered nanographites with metallic potassium under the same conditions as used to produce a stage 1 intercalation compound of bulk graphite with potassium is a mixture of nanographites and stage 1, stage 2, and stage 3 NGIC.[82] In the stage 1 NGIC with potassium, the charge transfer to the carbon network is lower by a factor of 2.5 than that in the stage 1 compound of bulk graphite with the same element (an electron per ~33 (see Ref. 82) and ~13 carbon atoms,[93] respectively).

When weak electron acceptors like iodine and bromine are intercalated in nanographite, the shift of the Fermi level does not exceed the width of the edge π-electron zone.[80–82] In nanographite with intercalated potassium atoms, the Fermi level is shifted beyond the edge π-electron zone and, accordingly, its effect on the properties of the nanoparticle diminishes appreciably.[81] The ESR spectrum of the NGIC with bromine and iodine shows no CESR signal, while the magnetic resonance on delocalized electrons in the NGIC with potassium is easily detected,[81] although the shift of the Fermi level in the latter is more considerable than that in the former. The observed difference in the magnetic properties of the NGIC with potassium and these halogens can be explained by considering some admixture of the wave functions of the "guest" molecules in the wave function of the conduction electrons of the matrix. Since spin—orbital interactions in bromine and iodine atoms are much stronger than those in potassium atoms, such an admixture should obviously increase the spin relaxation rate of the carriers in the NGIC with halogens to such an extent that precludes a CESR signal from being detected by standard methods. Note that for intercalation compounds of bulk graphite with electron acceptors, this situation is an exception rather than a rule.[93,96] Data for NGIC with electron acceptors are still insufficient even for making such conclusions.

Bulk graphite is a hydrophobic material, so it forms no intercalation compounds with water. However, since hydrophobicity may be thought of as a low degree of hydrophilicity, intermolecular attractive forces will always act, to some or other extent, between the molecules of water and any solid, including graphite. The only question arises as to whether these weak interactions can cause detected changes in the properties of a carbon material involved. This question is already answered for some nanoscale carbon systems. For instance, water molecules adsorbed on a single-walled carbon nanotube (a rolled graphene sheet) have been found to substantially increase the emission current[97] and decrease its hole conductivity.[98] According to the calculations,[99] the revealed changes in the properties of nanotubes can be explained by a transfer of an electron per ~33 adsorbed water molecules. An interaction of ACF with water molecules also changes the structure and magnetic properties of nanographites.[42,43,100,101]

In water-saturated ACF, the (002) reflection in X-ray diffraction experiments is observed at a larger 2θ value compared to both the starting dry fiber and bulk regular graphite (Fig. 13).[42,43] The new position of the (002) re-

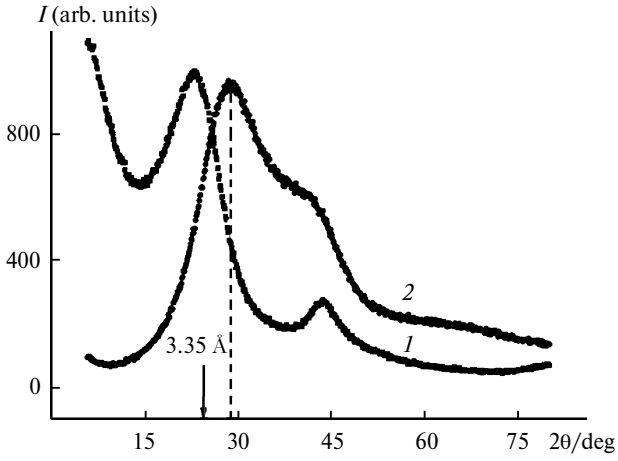

Fig. 13. Shift of the (002) reflection from ACF upon the water sorption:[42,43] (*1*) the initial sample and (*2*) the sample with sorbed water. The arrow indicates the position of the (002) reflection for bulk graphite.

flection for the fiber with sorbed water molecules indicates the changed identity period of nanographites along the direction perpendicular to the nanographene planes. However, since this signal is wide, one cannot specify when the (002) reflection shifts to the new position and when it disappears without any shift, but with a new reflection appearing on its branch at a different 2θ value. If the changed position of the (002) reflection (see Fig. 13) is considered resulting from its continuous shift, then its new 2θ value corresponds to the spacing $d_c = 0.322 \pm 0.005$ nm between the carbon layers in nanographites. This spacing is appreciably smaller than that in bulk regular graphite ($d_c = 0.335 \pm 0.001$ nm). To compress bulk graphite to this d_c value, the applied axial pressure must be ~40 kbar.[102] The formation of such a high pressure in ACF micropores (*e.g.*, as a result of water solidification) is very unlikely because of the degradation of ACF in this case, which has never been observed even upon the repeated cycles of water sorption—desorption. Therefore, the reflection at $2\theta \approx 29°$ (see Fig. 13) for water-saturated ACF is a new reflection corresponding to $d_c = (0.322 \pm 0.005) \times 2 = 0.64 \pm 0.01$ nm. Such a considerable spacing between the carbon layers in nanographite can be explained only by intercalation of water molecules. According to the calculations,[103] the planes of water molecules and nanographenes should be nearly perpendicular to each other at this d_c value.

The data from ESR spectroscopy and magnetic susceptibility measurements suggest that adsorbed water molecules largely suppress the ACF paramagnetism mainly due to the edge π-electron states of nanographites.[100] Taking into account the accompanying structural changes in both nanographites themselves and their disordered system, one can interpret this result as the transition (crossover) of the disordered 3D network of nanographites from the paramagnetic to low-spin state.[100]

As with water-saturated ACF, the (002) reflection from ACF exposed to fuming HNO_3 for ~0.1 h appears in the X-ray diffraction spectrum at a greater 2θ value compared to the spectrum of the initial fibers. This result is surprising because the density of HNO_3, in contrast to water, increases upon its crystallization (the acid becomes "compressed"). In this sense, its possible solidification in ACF micropores cannot, even hypothetically, give rise to high pressures affecting graphite nanoparticles (the walls of micropores). If the (002) reflection from HNO_3-saturated ACF is considered a new one, then the corresponding d_c value should be 0.73 ± 0.02 nm. Note that this spacing is intermediate between the d_c values in the α- and β-modifications of the intercalation compound of bulk graphite with HNO_3 (~0.78 and ~0.66 nm, respectively).[93,104] A detailed study[83] of the interaction of ACF with the vapor of fuming HNO_3 has revealed that a charge transfer first involves the outer faces of nanographites (they simultaneously function as the walls of micropores). As acid molecules become intercalated between the carbon layers of nanographites, the charge transfer involves their inner layers as well.

It is well known[105] that under normal conditions nanographite binds lithium ions three times greater than bulk graphite does. This enhanced ability of nanographite to attach lithium ions can easily be explained[106,107] by considering its edge π-electron states. Indeed, for a lithium atom in the vicinity of the zigzag edge of nanographite with the saturated σ-orbitals, there is some probability of a charge transfer to the edge π-electron states whose energies are close to the Fermi level but somewhat lower than the energy of the 2s orbital of the lithium atom.[107] In other words, nanographite can combine with lithium to give a specific edge charge-transfer compound.

Thus, nanographene is an intermediate between graphene and aromatic molecules. However, some properties of nanographene are unique, being exhibited by neither graphene nor aromatic molecules. For this reason, nanographenes and their stacks (nanographites) can be regarded as individual nanocarbon systems possessing characteristic physical and chemical properties.

Investigations of nanographites are of considerable theoretical and applied interest. Theoretically, these objects are nanoscale π-electron conjugated systems with open edges and thus differ in reactivity from bulk graphite. This allows the synthesis of specific nanographite compounds in which the carbon—element bonding occurs mainly at the periphery of a nanoparticle. In addition, the specific peripheral π-electron states in nanographites with predominant zigzag edges are responsible for their unusual electronic structures near the Fermi level as well as for their unconventional physical and chemical properties. For this reason, nanographites have become a subject of extensive studies aimed at revealing their new features and peculiar manifestations of their known properties in some or other situations. Specific topics of great interest include the growing of nanographites with particular edge patterns, the design and study of nanographites with the chemically nonequivalent states of their opposite edges, the synthesis of intercalation and edge compounds of nanographite with lithium, the preparation and examination of chain structures at the nanographite edges, the growing and study of nanographite films and novel composite materials with nanographite as a filler.

The problems associated with the synthesis and study of nanographites and their compounds, films, and composites adjoin those in their practical application. The solution of these problems depends in turn on the production cost of nanographites, including nanoparticles with controlled edge size and shapes, which is currently still

high. Nevertheless, the subminiature sizes, good conductivity, high emission parameters, nonlinear optical characteristics, and unusual magnetic properties of nanographites make them promising for use in nanoelectronics, measuring instruments, chemical technology, and energy storage applications; this will be another example of the efficient impact of basic research on scientific and technical progress.

This work was financially supported by the Presidium of the Russian Academy of Sciences and the Presidium of the Far East Branch of the Russian Academy of Sciences (Joint Project No. 12-I-P8-10), the Division of Chemistry and Materials Science of the Russian Academy of Sciences and the Presidium of the Far East Branch of the Russian Academy of Sciences (Joint Project No. 12-I-OKhNM-03), and the Presidiums of the Siberian and Far East Branches of the Russian Academy of Sciences (Project No. 12-II-SO-04-011).

References

1. M. S. Dresselhaus, G. Dresselhaus, P. C. Ekland, *Science of Fullerenes and Carbon Nanotubes*, Academic Press, New York, 1996, 368 pp.
2. A. H. Castro Neto, F. Guinea, N. M. R. Peres, K. S. Novoselov, A. K. Geim, *Rev. Mod. Phys.*, 2009, **81**, 109.
3. A. Krueger, *Carbon Materials and Nanotechnology*, Wiley-VCH, Weinheim (Germany), 2010, 475 pp.
4. T. Enoki, T. Ando, *Physics and Chemistry of Graphene*: *Graphene to Nanographene*, Pan Stanford Publishing Pte Ltd., Singapore, 2013, 476 pp.
5. H. Marsh, F. Rodriguez-Reinoso, *Activated Carbon*, Elsevier, Amsterdam, 2006, 536 pp.
6. H. Fujimoto, *Carbon*, 2003, **41**, 1585.
7. N. S. Saenko, A. M. Ziatdinov, *Izv. Vyssh. Uchebn. Zaved., Khim. Khim. Tekhnol.* [*Bulletin of High Schools, Chemistry and Chemical Technology*], 2013, **56**, No. 7, 46 (in Russian).
8. K. Kaneko, C. Ishii, M. Ruike, H. Kuwabara, *Carbon*, 1992, **30**, 1075.
9. C. Ishiii, Y. Matsumura, K. Kaneko, *J. Phys. Chem.*, 1995, **99**, 5743.
10. M. Sato, H. Isobe, K. Yamamoto, T. Iiyama, K. Kaneko, *Carbon*, 1995, **33**, 1347.
11. S. Welz, M. McNallan, Y. Gogotsi, *J. Mater. Process. Technol.*, 2006, **179**, 11.
12. A. E. Kravchenko, Yu. A. Kukushkina, V. V. Sokolov, G. F. Tereshchenko, E. A. Ustinov, *Russ. J. Appl. Chem.* (*Engl. Transl.*), 2008, **81**, 1733 [*Zh. Prikl. Khim.*, 2008, **81**, 1605].
13. L. A. Aleshina, D. V. Loginov, A. D. Fofanov, R. N. Kyutt, *Russ. J. Solid State Phys.* (*Engl. Transl.*), 2011, **53**, 1739 [*Fiz. Tverd. Tela*, 2011, **53**, 1651].
14. A. Nakayama, K. Suzuki, N. Enoki, K.-I. Koga, M. Endo, N. Shindo, *Bull. Chem. Soc. Jpn*, 1996, **69**, 333.
15. V. Yu. Osipov, T. Enoki, K. Takai, K. Takahara, M. Endo, T. Hayashi, Y. Hishiyama, Y. Kaburagi, A. Ya. Vul´, *Carbon*, 2006, **44**, 1225.
16. J. Qiu, Y. Li, Y. Wang, C. Liang, T. Wang, D. Wang, *Carbon*, 2003, **41**, 767.
17. M. S. Akhter, A. R. Chunghtai, D. M. Smith, *Appl. Spectrosc.*, 1985, **39**, 143.
18. N. Fernandez-Alos, J. K. Watson, R. L. Vander Wal, J. P. Mathews, *Combust. Flame*, 2011, **158**, 1807.
19. J. D. Kubicki, *Geochem. Trans.*, 2000, **7**, 41.
20. A. M. Affoune, B. L. V. Prasad, H. Sato, T. Enoki, Y. Kaburagi, Y. Hishiyama, *Chem. Phys. Lett.*, 2001, **348**, 17.
21. K. Harigaya, Y. Kobayashi, K. Takai, J. Ravier, T. Enoki, *J. Phys.: Condens. Matter*, 2002, **14**, L605.
22. M. Fujita, K. Wakabayashi, K. Nakada, K. Kusakabe, *J. Phys. Soc. Jpn*, 1996, **65**, 1920.
23. K. Nakada, M. Fujita, G. Dresselhaus, M. S. Dresselhaus, *Phys. Rev. B: Condens. Matter*, 1996, **54**, 17954.
24. K. Wakabayashi, M. Fujita, H. Ajiki, M. Sigrist, *Phys. Rev. B: Condens. Matter*, 1999, **59**, 8271.
25. T. Enoki, *Phys. Scr.*, 2012, **146**, 014008.
26. M. Fujita, M. Igami, K. Nakada, *J. Phys. Soc. Jpn*, 1997, **66**, 1864.
27. C. P. Chung, C. L. Lu, F. L. Shyu, R. B. Chen, Y. C. Huang, M. F. Lin, *Carbon*, 2005, **43**, 1424.
28. K. Harigaya, T. Enoki, *Chem. Phys. Lett.*, 2002, **351**, 129.
29. F. L. Shyu, M. F. Lin, *Physica E*, 2003, **16**, 214.
30. P. Koskinen, S. Malola, H. Hakkinen, *Phys. Rev. Lett.*, 2008, **101**, 115502.
31. B. Huang, M. Lin, N. Su, J. Wu, W. Duan, B.-I. Gu, F. Lin, *Phys. Rev. Lett.*, 2009, **102**, 166404.
32. Y. Lin, A. Dobrinsky, B. I. Yakobson, *Phys. Rev. Lett.*, 2010, **105**, 235502.
33. D. Wei, F. Wang, *Surf. Sci.*, 2012, **606**, 485.
34. S. Fujii, T. Enoki, *J. Am. Chem. Soc.*, 2010, **132**, 10034.
35. US Pat. 20130108839 (02/05/2013); *Chem. Abstrs*, 2013, **158**, 623038.
36. Y. Niimi, T. Matsui, H. Kambara, K. Tagami, M. Tsukada, H. Fukuyama, *Appl. Surf. Sci.*, 2005, **241**, 43.
37. Y. Kobayashi, K. Fukui, T. Enoki, K. Kusakabe, Y. Kaburagi, *Phys. Rev. B: Condens. Matter*, 2005, **71**, 193406.
38. Z. Klusek, W. Kozlowski, Z. Waqar, S. Datta, J. S. Burnell-Gray, I. V. Makarenko, N. R. Gall, E. V. Rutkov, A. Ya. Tontegode, A. N. Titkov, *Appl. Surf. Sci.*, 2005, **252**, 1221.
39. M. Ziatdinov, S. Fujii, K. Kusakabe, M. Kiguchi, T. Mori, T. Enoki, *Phys. Rev. B: Condens. Matter*, 2013, **87**, 115427.
40. S. Fujii, M. Ziatdinov, K. Kusakabe, M. Kiguchi, T. Enoki, *Faraday Discuss.*, 2014, **173**, No. 12, 173.
41. M. Ohtsuka, S. Fujii, M. Kiguchi, T. Enoki, *ACSNano*, 2013, **7**, 6868.
42. A. M. Ziatdinov, *Ross. Khim. Zh.*, 2004, **47**, No. 5, 5 [*Mendeleev Chem. J.* (*Engl. Transl.*), 2004, **47**, No. 5].
43. A. M. Ziatdinov, in *Nanostructures: Physics and Technology*, Eds Zh. Alferov, L. Esaki, Academic University, St. Petersburg, 2010, 168.
44. V. L. J. Joly, M. Kiguchi, S.-J. Hao, K. Takai, T. Enoki, R. Sumii, K. Amemiya, H. Muramatsu, T. Hayashi, Y. A. Kim, M. Endo, J. Campos-Delgado, F. Lopez-Urias, A. Botello-Mendez, H. Terrones, M. Terrones, M. S. Dresselhaus, *Phys. Rev. B: Condens. Matter*, 2010, **81**, 245428.
45. M. Kiguchi, K. Takai, V. L. J. Joly, T. Enoki, R. Sumii, K. Amemiya, *Phys. Rev. B: Condens. Matter*, 2011, **84**, 045421.

46. S. Entan, S. Ikeda, M. Kiguchi, K. Saiki, G. Yoshikawa, I. Nakai, H. Kondoh, T. Ohta, *Appl. Phys. Lett.*, 2006, **88**, 153126.
47. J. Weil, J. R. Bolton, *Electron Paramagnetic Resonance: Elementary Theory and Practical Applications*, Wiley-Interscience, New Jersey, 2007, 664 pp.
48. J. Tian, H. Cao, W. Wu, Q. Yu, Y. P. Chen, *Nano Lett.*, 2011, **11**, 3663.
49. M. Yamamoto, S. Obata, K. Saiki, *Surf. Interface Anal.*, 2010, **42**, 1637.
50. D. Sabramanian, F. Libisch, Y. Li, C. Pauly, V. Geringer, R. Reiter, T. Mashoff, M. Liebmann, J. Burgdorfer, C. Busse, T. Michely, R. Mazzarello, M. Pratzer, M. Morgenstern, *Phys. Rev. Lett.*, 2012, **108**, 046801.
51. S. K. Hamalainen, Z. Sun, M. P. Boneschanscher, A. Uppstu, M. Ijas, A. Harju, D. Vanmaekelbergh, P. Liljeroth, *Phys. Rev. Lett.*, 2011, **107**, 236803.
52. G. O. Girit, J. C. Meyer, R. Erni, M. D. Rossell, C. Kisielovski, L. Yang, C.-H. Park, M. F. Crommie, M. L. Cohen, S. G. Louie, A. Zettl, *Science*, 2009, **323**, 1705.
53. A. Nakayama, K. Suzuki, T. Enoki, S. L. di Vittorio, M. S. Dresselhaus, K. Koga, M. Endo, N. Shindo, *Synth. Met.*, 1993, **57**, 3736.
54. Y. Shibayama, H. Sato, T. Enoki, M. Endo, *Phys. Rev. Lett.*, 2000, **84**, 1744.
55. G. A. Petrakovskii, *Usp. Fiz. Nauk*, 1981, **134**, 305 [*Sov. Phys. Usp.* (*Engl. Transl.*), 1981, **24**, 511].
56. G. M. Mikheev, R. G. Zonov, A. N. Obraztsov, A. P. Volkov, Yu. P. Svirko, *Instrum. Exp. Tech.* (*Engl. Transl.*), 2005, **48**, 349 [*Prib. Tekh. Eksp.*, 2005, **48**, 84].
57. G. M. Mikheev, R. G. Zonov, A. N. Obraztsov, Yu. P. Svirko, *Tech. Phys. Lett.* (*Engl. Transl.*), 2004, **30**, 750 [*Pisma Zh. Tekh. Fiz.*, 2004, **30**, 88].
58. G. M. Mikheev, R. G. Zonov, A. N. Obraztsov, V. M. Styapshin, *Tech. Phys. Lett.* (*Engl. Transl.*), 2008, **34**, 467 [*Pisma Zh. Tekh. Fiz.*, 2008, **34**, 29].
59. A. N. Obraztsov, A. P. Volkov, A. A. Zakhidov, *Appl. Surf. Sci.*, 2003, **215**, 214.
60. A. N. Obraztsov, V. I. Kleshch, E. A. Smolnikova, *Beilstein J. Nanotechnol.*, 2013, **4**, 493.
61. S. G. Lebedev, *Adv. High Energy Phys.*, 2013, **2013**, 612582.
62. S. G. Lebedev, V. E. Yants, A. S. Lebedev, *Nucl. Instrum. Methods Phys. Res., Sect. A*, 2008, **590**, 227.
63. S. G. Lebedev, *Unconventional Electromagnetics in Carbonaceous Materials*, Nova Science Publishers, New York, 2010, 107 pp.
64. Yu. V. Ioni, S. V. Tkachev, N. A. Bulychev, S. P. Gubin, *Inorg. Mater.* (*Engl. Transl.*), 2011, **47**, 597 [*Neorg. Mater.*, 2011, **47**, 671].
65. A. Serra, A. Buccolieri, E. Filippo, D. Manno, *Sens. Actuators, B*, 2012, **161**, 359.
66. US Pat. 8226801 (24/07/2012); *Chem. Abstr*s, 2011, **154**, 172031.
67. S. Mitani, M. Sathish, D. Rangappa, A. Unemoto, T. Tomai, I. Honma, *Electrochim. Acta*, 2012, **68**, 146.
68. A. M. Ziatdinov, *Izv. Vyssh. Uchebn. Zaved., Khim. Khim. Tekhnol.* [*Bulletin of High Schools, Chemistry and Chemical Technology*], 2013, **56**, No. 7, 3 (in Russian).
69. A. M. Ziatdinov, in *Perspektivnye napravleniya razvitiya nanotekhnologii v DVO RAN* [*Promising Avenues for the Development of Nanotechnology in the Far East Branch of the Russian Academy of Sciences*], Ed. Yu. M. Kul´chin, Dal´nauka, Vladivostok, 2013, p. 54 (in Russian).
70. C. Jo, S. An, Y. Kim, J. Shim, S. Yoon, J. Lee, *Phys. Chem. Chem. Phys.*, 2012, **14**, 5695.
71. A. Bhattacharyya, M. Joshi, *Int. J. Nanosci.*, 2011, **19**, 1125.
72. M. Li, *Appl. Energy*, 2013, **106**, 25.
73. D. Bansal, S. Pillay, U. Vaidya, *Carbon*, 2013, **55**, 233.
74. E. J. E. Stuart, M. Pumera, *J. Phys. Chem. C*, 2011, **115**, 5530.
75. L. R. Zhao, B. Z. Jang, *J. Mater. Sci. Lett.*, 1996, **15**, 99.
76. T. Enoki, Y. Kobayashi, K.-I. Fukui, *Int. Rev. Phys. Chem.*, 2007, **26**, 609.
77. Yu. M. Nikolenko, A. M. Ziatdinov, *Russ. J. Inorg. Chem.* (*Engl. Transl.*), 2012, **57**, 1436 [*Zh. Neorg. Khim.*, 2012, **57**, 1528].
78. X. Sun, Z. Lin, K. Welsher, J. T. Robinson, A. Goodwin, S. Zaric, H. Dai, *Nano Res.*, 2008, **1**, 203.
79. X. Zhan, S. Wang, M. Liu, B. Yang, L. Feng, Y. Ji, L. Tao, Y. Wei, *Phys. Chem. Chem. Phys.*, 2013, **15**, 19013.
80. Y. Shibayama, H. Sato, T. Enoki, *Mol. Cryst. Liq. Cryst.*, 2000, **340**, 301.
81. B. L. V. Prasad, H. Sato, T. Enoki, Y. Hishiyama, Y. Kaburagi, A. M. Rao, G. U. Sumanasekera, P. C. Eklund, *Phys. Rev. B: Condens. Matter*, 2001, **64**, 235407.
82. K. Takai, H. Kumagai, H. Sato, T. Enoki, *Phys. Rev. B: Condens. Matter*, 2006, **73**, 035435.
83. S.-J. Hao, K. Takai, J. V. L. Joly, T. Enoki, *J. Phys. Chem. Solids*, 2012, **73**, 1432.
84. D.-E. Jiang, B. G. Sumpter, S. Dai, *J. Chem. Phys.*, 2007, **126**, 134701.
85. R. Saito, M. Yagi, T. Kimura, G. Dresselhaus, M. S. Dresselhaus, *J. Phys. Chem. Solids*, 1999, **60**, 715.
86. T. Wassmann, A. P. Seitsonen, A. M. Saitta, M. Lazeri, F. Mauri, *Phys. Rev. Lett.*, 2008, **101**, 096402.
87. N. Watanabe, T. Nakajima, H. Touhara, *Graphite Fluorides*, Elsevier, Amsterdam, 1988, 263 pp.
88. Q. Chen, X. Wang, Z. Wang, Y. Liu, T. You, *Nanoscale Res. Lett.*, 2013, **8**, 52.
89. S. P. Gubin, Yu. A. Koksharov, G. B. Homutov, G. Yu. Yurkov, *Russ. Chem. Rev.*, 2005, **74**, 489.
90. K. Kusakabe, M. Maruyama, *Phys. Rev. B: Condens. Matter*, 2003, **67**, 092406.
91. M. Maruyama, K. Kusakabe, S. Tsuneyuki, K. Akagi, Y. Yoshihide, J. Yamauchi, *J. Phys. Chem. Solids*, 2004, **65**, 119.
92. N. Gorjizadeh, Y. Kawazoe, *J. Nanomater.*, 2010, **2010**, 513501.
93. M. S. Dresselhaus, G. Dresselhaus, *Adv. Phys.*, 1981, **30**, 139.
94. Z. Buffet, *Properties of the Perylene Iodine Complex*, McMaster University, Canada, 1997, 142 pp.
95. L. Grigorian, K. A. Williams, S. Fang, *Phys. Rev. Lett.*, 1998, **80**, 5560.
96. A. M. Ziatdinov, *Mol. Phys. Rep.*, 1997, **18/19**, 149.
97. K. A. Dean, P. von Allmen, B. R. Chalamala, *J. Vac. Sci. Technol., B*, 1999, **17**, 1959.
98. A. Zahab, L. Spina, P. Poncharal, C. Marliere, *Phys. Rev. B: Condens. Matter*, 2000, **62**, 10000.
99. R. Pati, Y. Zhang, S. K. Nayak, *Appl. Phys. Lett.*, 2002, **81**, 2638.

100. H. Sato, N. Kawatsu, T. Enoki, M. Endo, R. Kobori, M. Satoshi, K. Kaneko, *Solid State Commun.*, 2003, **125**, 641.
101. M. Sliwinska-Bartkowiak, H. Drozdowski, M. Kempinski, M. Jazdzewska, Y. Long, J. C. Palmer, K. E. Gubbins, *Phys. Chem. Chem. Phys.*, 2012, **14**, 7145.
102. R. Clarke, C. Uher, *Adv. Phys.*, 1984, **33**, 469.
103. H. Ruuska, T. A. Pakkanen, *Carbon*, 2003, **41**, 699.
104. A. M. Ziatdinov, N. M. Mishchenko, *Solid State Commun.*, 1996, **97**, 1085.
105. K. Sato, M. Noguchi, A. Demachi, N. Oki, M. Endo, *Science*, 1994, **264**, 556.
106. M. Nakadaira, R. Saito, T. Kimura, G. Dresselhaus, M. S. Dresselhaus, *J. Mater. Res.*, 1997, **12**, 1367.
107. M. Yagi, R. Saito, T. Kimura, G. Dresselhaus, M. S. Dresselhaus, *J. Mater. Res.*, 1999, **14**, 3799.

Received February 11, 2014;
in revised form July 28, 2014